



HAL
open science

Properties of metastable linkage NO isomers in $\text{Na}_2[\text{Fe}(\text{CN})_5\text{NO}] \times 2\text{H}_2\text{O}$ incorporated in mesopores of silica xerogels

Zakaria Tahri, Robert Lepski, Kuan-Ying Hsieh, El-Eulmi Bendeif, Sebastien Pillet, Pierrick Durand, Theo Woike, Dominik Schaniel

► To cite this version:

Zakaria Tahri, Robert Lepski, Kuan-Ying Hsieh, El-Eulmi Bendeif, Sebastien Pillet, et al.. Properties of metastable linkage NO isomers in $\text{Na}_2[\text{Fe}(\text{CN})_5\text{NO}] \times 2\text{H}_2\text{O}$ incorporated in mesopores of silica xerogels. *Physical Chemistry Chemical Physics*, 2012, 14 (11), pp.3775-3781. 10.1039/c2cp23607a . hal-04398349

HAL Id: hal-04398349

<https://hal.science/hal-04398349>

Submitted on 23 Jan 2024

HAL is a multi-disciplinary open access archive for the deposit and dissemination of scientific research documents, whether they are published or not. The documents may come from teaching and research institutions in France or abroad, or from public or private research centers.

L'archive ouverte pluridisciplinaire **HAL**, est destinée au dépôt et à la diffusion de documents scientifiques de niveau recherche, publiés ou non, émanant des établissements d'enseignement et de recherche français ou étrangers, des laboratoires publics ou privés.

Properties of metastable linkage NO isomers in $\text{Na}_2[\text{Fe}(\text{CN})_5\text{NO}]\cdot 2\text{H}_2\text{O}$ incorporated in mesopores of silica xerogels[‡]

Zakaria Tahri,^a Robert Lepski,^b Kuan-Ying Hsieh,^a El-Eulmi Bendeif,^a Sebastien Pillet,^a Pierrick Durand,^a Theo Woike^c and Dominik Schaniel^{*a}

Received Xth XXXXXXXXXX 20XX, Accepted Xth XXXXXXXXXX 20XX

First published on the web Xth XXXXXXXXXX 200X

DOI: 10.1039/b000000x

We study the properties of photoinduced metal-nitrosyl linkage isomers in sodium nitroprusside (SNP) as a function of particle size. By embedding the molecular complex in various concentrations into mesopores of silica xerogels the size of the particles can be adjusted. The ground state is characterized by X-ray diffraction, absorption and infrared spectroscopy. The physical properties of the photoswitched molecules were analysed by steady-state low-temperature absorption, infrared spectroscopy and by nanosecond transient absorption spectroscopy. The electronic structure as well as the activation energies of the metastable linkage isomers are independent of the particle size down to single isolated molecules, indicating that the SNP complexes are quasi-free inside the pores of the gel.

1 Introduction

The generation of photoinduced nitrosyl linkage isomers in $\text{Na}_2[\text{Fe}(\text{CN})_5\text{NO}]\cdot 2\text{H}_2\text{O}$ (SNP) is connected with a photochromic and photorefractive response of the material which renders it interesting for optical applications^{1–6}. Such applications would demand a more robust and industrial processing than growing single crystals. A potential route to applicable materials is the embedding of the complex into polymers or sol-gel based materials like silica or titania matrices or the deposition on functionalized surfaces^{7–20}. From a fundamental point of view it is interesting to study the properties of the complex and its photoinduced linkage isomers as a function of particle size and variation of the environment. First studies of $(\text{CN}_3\text{H}_6)_2[\text{Fe}(\text{CN})_5\text{NO}]$ embedded in bulk silica xerogels indicated that the structure of the complex remains close to that found in single crystals²¹ and that the $[\text{Fe}(\text{CN})_5\text{NO}]$ -molecule retains its ability to form linkage isomers¹¹. In the case where the molecule is electrostatically attached to thin films of mesoporous TiO_2 deposited on silicon, the photofunctionality is changed towards a release of the NO and CN ligands upon irradiation¹³. These different functionalities depend on the electronic structure and on the

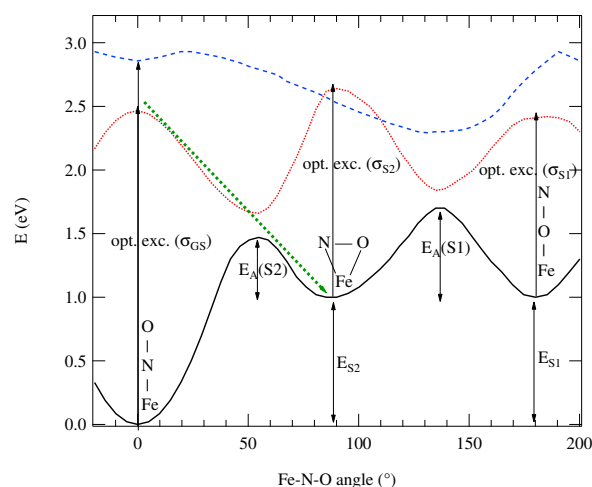


Fig. 1 Potential scheme illustrating the characteristic points of the potential surface and relaxation pathways during generation of linkage isomers in ML_5NO compounds²².

characteristics of the potential energy surface. The generation of linkage isomers in such $\text{X}_n[\text{ML}_5\text{NO}]\text{yH}_2\text{O}$ complexes with different transition metals M such as nickel^{23,24}, ruthenium^{25–29}, osmium³⁰, iron³¹, platinum^{32,33}, different ligands L such as F, Cl, Br, I, OH, CN, NH_3 , NO_2 , pyridine, different counter ions X_n such as (CN_3H_6) , alkali, earth alkali, halogen, NH_4 , and different amounts y of crystal water³⁴ can be described in a generalized potential scheme as illustrated in Fig. 1²². The optical excitation leads to a change in the bond between the central metal atom M and the NO ligand which

^a CRM2 UMR 7036, Institut Jean Barriol, Nancy Université, BP 70239, 54506 Vandoeuvre les Nancy, France. Fax: 0033 383 684300; Tel: 0033 383684889; E-mail: dominik.schaniel@crm2.uhp-nancy.fr

^b I. Physikalisches Institut, Universität zu Köln, Zùlpicher Str. 77, 50674 Köln, Germany.

^c Institut für Strukturphysik, TU Dresden, Zellescher Weg 16, Dresden, Germany.

[‡] Financial support by the BMBF (FKZ 03X5510) and DFG (SCHA1550/1-1) is gratefully acknowledged.

triggers the rotation of the NO group. If the excited state potential possesses a minimum close to the saddle point of the ground state surface between the ground state (GS) and the metastable states S1 or S2 or crosses that surface, the relaxation towards S1 or S2 can occur. It was recently shown that the relaxation into S2 occurs with a time constant of 200 femtoseconds³⁵. The NO ligand rotates from the N-bound configuration (M-N-O) in GS either to the O-bound configuration M-O-N (S1) by nearly 180° or by about 90° to the side-on bound configuration $M \leftarrow O_N$ (S2)^{36–38}. These new structures correspond to two different potential minima (S1, S2) in the relaxed GS potential^{22,39,40}. In SNP the linkage isomers are separated from the GS by potential barriers of $E_A = 0.68$ eV (S1) and $E_A = 0.47$ eV (S2), so that at low temperatures they exhibit lifetimes $t > 10^6$ s⁴¹. At low temperature the population, i.e. number of transferred molecules into S1 or S2, depends on the absorption cross sections $\sigma_{GS,S1,S2}$ for population and depopulation that establish the photostationary state. In order to explore the properties of isolated ML₅NO molecules and the generation conditions of photoinduced linkage isomers in these conditions we studied the electronic structure and potential energy surface of SNP embedded in silica xerogels using X-ray diffraction, absorption and infrared spectroscopy, and transient transmission measurements.

2 Experimental details

2.1 Synthesis of Silica-SNP hybrids

Silica-SNP hybrids were prepared following the two slightly different procedures described hereafter.

1. Procedure A: 1.5 ml of Tetramethoxysilane (TMOS, 98% purity, Fluka), 1.8 ml of methanol (VWR) and 3.6 ml of distilled water were mixed and stirred for 5 minutes which allowed the solution to gel. Then 3.1 ml of two different concentrations (0.1 mol L⁻¹ and 0.01 mol L⁻¹) of aqueous SNP solutions were added and stirred for another 5 minutes in the glass dish. The mixtures were kept at 50°C for 7 days in an oven and dried at room temperature in air for 1 week. The resulting SNP concentrations were 310 and 31 μmol per gel.
2. Procedure B: 1.5 ml of TMOS, 1.8 ml of methanol (VWR) and 3.6 ml of distilled water and different amounts of 0.25 mol L⁻¹ aqueous SNP solutions were mixed and stirred for about 30 minutes. The amount of water was kept constant at 3.6 ml, e.g., when 2.0 ml of aqueous SNP solution were added only 1.6 ml of pure H₂O was added. By variation of the amount of added SNP solution the concentration of SNP was varied between 12.5 and 875 μmol per gel. After the 30 minutes the gels in the glass dish were covered by parafilm or a

cap and put for 1 week into a dry chamber at 50°C in order to allow for complete gelation. Then small holes were pierced into the parafilm or the cap in order to allow for a complete evaporation of remaining solvents in about 1 week. Then the parafilm or cap was completely removed and the gel dried for a further 4-8 weeks in the dry cabinet. Finally the dried gels were put in an exsiccator at 10⁻³ mbar in order to remove remaining solvent molecules.

2.2 X-Ray diffraction

X-ray powder diffraction measurements were performed on a PANalytical XPert system equipped with a reflection spinner, scanning 2θ from 5 to 68 degree using Cu K α_1 radiation ($\lambda = 1.5406$ Å). The particle size L of embedded nanoparticles of SNP was determined from the broadening of the Bragg peaks according to Scherrers formula $\Delta(2\theta) = K/\lambda \cos \theta_0$ using the Scherrer factor $K = 0.9$ for the Bragg peak at $2\theta_0 = 30.9^\circ$ corresponding to $Q = 4\pi \sin \theta_0/\lambda = 2.173$ Å⁻¹ (see Fig. 2).

2.3 UV/Vis and infrared spectroscopy

UV-Vis absorption spectra were recorded with a Shimadzu UV-3600 UV-Vis-NIR spectrophotometer. For the low-temperature measurements a home-built cryostat was used, where the sample is positioned in a N₂ gas atmosphere. The double-walled cryostat is equipped with glass windows that allow for measurement and in-situ illumination of the samples. The molar extinction coefficient $\epsilon(\lambda)$ was determined according to the Lambert-Beer law $E(\lambda) = -\lg(I/I_0) = \alpha(\lambda)d = \epsilon(\lambda)cd$, where $E(\lambda)$ denotes the measured absorption, I and I_0 the intensity of the probe and reference beam, c the concentration of SNP complexes in the sample, and d the thickness of the sample. Knowing the volume of the prepared disk-like samples (procedure B) $V_{Gel} = \pi r^2 d$, r being the radius of the disk and d the thickness, the concentration of samples is given by $c = n/V_{Gel}$, n being the number of moles per gel, as indicated above. The infrared spectra were collected with a Nicolet 5700 FTIR spectrometer and a resolution of 2 cm⁻¹. The samples were finely ground, mixed with KBr, and pressed to pellets. To ensure good thermal contact for the low-temperature measurements the pellets were contacted with silver paste on the cold finger of a home-built cryostat. The samples are cooled to liquid nitrogen temperature (80 K) in the evacuated sample chamber (10⁻⁶ mbar). The cryostat is equipped with CsI windows allowing for collection of spectra in the range 8000-260 cm⁻¹ and for in-situ illumination with lasers. The excitation of the samples at low temperature was performed with different laser sources with wavelengths ranging from 325 nm up to 1064 nm.

2.4 Time-resolved transmission measurements

The generation and relaxation of light-induced metastable states at different temperatures in a SNP crystal and the different SNP gels are measured by transient absorption spectroscopy with nanosecond time resolution. The pump pulses that excite the sample were provided by a SureliteTM laser with wavelength $\lambda_p = 532$ nm corresponding to the frequency doubled pulse of the fundamental at $\lambda = 1064$ nm, with a pulse duration of $\tau_p = 5$ ns. This pump pulse is guided by two mirrors and focussed by a lens in order to obtain a diameter of about $d_p = 0.4$ cm on the sample surface and an energy of 35 mJ per pulse. The pump laser pulse is delivered on demand by an external control. The probe light was provided by a cw He-Ne laser centred at 632.8 nm that was focussed by a lens to a spot size much smaller than the pump pulse in order to ensure proper overlap of the probe and pump pulse on the sample position. The probe light is detected by 200MHz Si-Pin diode from Femto Messtechnik GmbH. The output voltage of the detector is sampled using a 1.5-GHz oscilloscope (Lecroy Wavepro 715zi). The trigger is obtained from another fast Si-Pin diode (Thorlabs PE310) that detects a part of the reflected light from the first guiding mirror. In order to block the pump light a color filter RG610 (FGL610 Thorlabs) and an interference filter IR632.8 (Coherent, FWHM = 10 nm) are mounted in front of the probe diode, blocking the 532 nm light by 10^{-6} . The measurements are performed as a function of temperature in the range 190-290 K. For this reason, the samples are mounted on the cold finger of an Oxford Instruments cryostat in a sample holder sandwiched between two thin glass plates to ensure good thermal contact and plane surfaces. The optical absorption changes induced due to the excitation of metastable states are measured as $\alpha_{ti} = (1/d)\ln(I(t=0)/I(t))$, where d is the thickness of the sample and $I(t)$ and $I(t=0)$ are, respectively, the intensity of the probe beam measured after and before the pulse irradiation. A typical trace is obtained by averaging 100 acquisitions in order to improve the signal to noise ratio.

3 Experimental results and discussion

3.1 Structural characterization

The synthesized xerogels with embedded SNP were characterized by X-ray diffraction. The top panel of Fig. 2 shows the powder diffraction patterns for the two samples prepared according to procedure A. For the sample with higher concentration ($c = 0.1$ mol/L corresponding to 310 μmol SNP in the gel) Bragg peaks are clearly visible and can be attributed to the structure of SNP (orthorhombic, space group $Pnmm$)³⁶. The reference diffraction pattern of a SNP powder sample is indicated by dashed lines in Fig. 2. The peak positions of the parti-

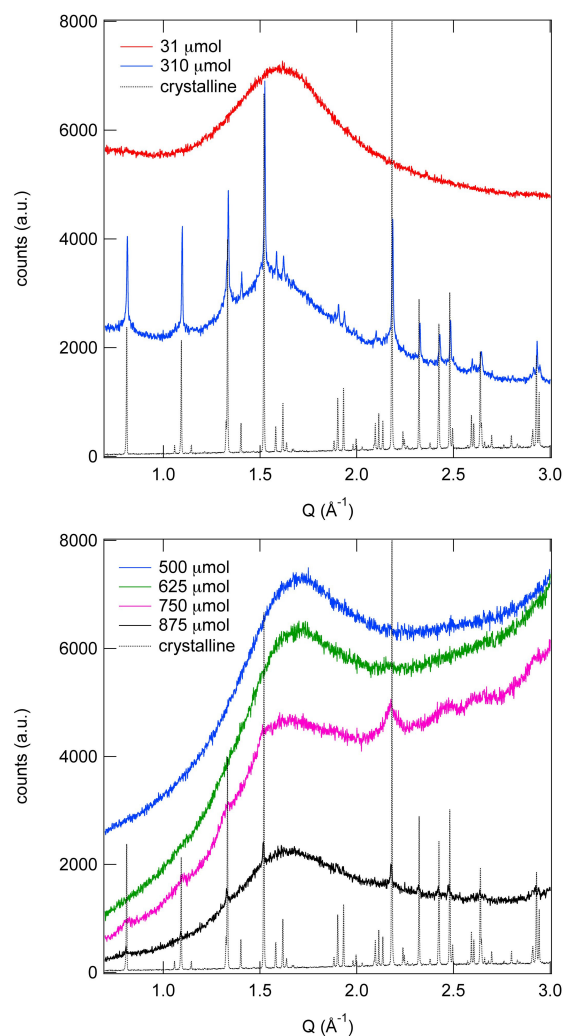


Fig. 2 X-ray diffraction pattern of xerogels with different concentrations of SNP synthesized according to procedures A (top) and B (bottom). With decreasing concentration the particle size of the embedded SNP decreases as can be seen from the broadening and subsequent disappearance of the Bragg peaks. The dotted line indicates the powder diffraction pattern of crystalline SNP.

cles formed within the gel and that of the crystalline reference sample coincide perfectly, clearly showing that the embedded particles exhibit the same structure as the crystalline phase of SNP. The peaks of the SNP xerogel sample are broadened and the evaluation of the broadening according to Scherrers formula yields a particle size of 83 nm. Note that this particle size corresponds to an average particle size. In fact the peaks exhibit an even more broadened base indicating the presence of particles smaller than 83 nm in the gel. The broad peak at $Q = 1.6 \text{ \AA}^{-1}$ is due to the amorphous SiO_2 matrix. For the sample with a ten times lower concentration ($c = 0.01 \text{ mol L}^{-1}$ corresponding to $31 \mu\text{mol}$ SNP in the gel) no traces of Bragg peaks could be detected, indicating that SNP is embedded as isolated complexes in the pores of the xerogel²¹. It is worth noting in this case that the amount of water used in the synthesis is identical for the two samples with different SNP concentrations; the porosity of the corresponding formed xerogel is thus expected to be quite similar and of the order of 1 nm^2 . As a consequence, the size of the embedded particles is independent of the pore size, indicating that the nanoparticles are formed before the xerogel matrix has become too rigid.

The bottom panel of Fig. 2 shows the powder diffraction patterns for four samples prepared according to procedure B with concentrations of 875, 750, 625, and $500 \mu\text{mol}$ per gel. The average particle size determined from the peak broadenings are 200 nm for a concentration of $875 \mu\text{mol}$ SNP per gel and 11 nm for $750 \mu\text{mol}$ SNP per gel. In the sample with $625 \mu\text{mol}$ SNP per gel the peaks are so broad that the analysis becomes difficult. An estimate yields particles of size 2-3 nm. At concentrations of $500 \mu\text{mol}$ and less SNP per gel no traces of Bragg peaks could be detected indicating again that SNP is embedded in the form of isolated complexes.

These structural measurements clearly show that the amount of initial concentration of SNP in the gel solution determines the particle size. For low enough concentrations the SNP complexes occur isolated in the pores of the xerogels, a result that is in agreement with previous studies^{11,21}. We note however that different procedures of sol-gel production lead to different results with respect to the size of embedded particles. By procedure A a concentration of $310 \mu\text{mol}$ SNP in the gel produces rather large particles of 83 nm, while the same concentration in procedure B results in isolated molecules in the gel. In procedure A the amount of H_2O used in the synthesis was superior compared to the procedure B (6.7 ml vs 3.1 ml). It is known that the gelation is slowed down when the amount of H_2O in the starting solution is increased. The SNP guest has thus more time to crystallize in procedure A, a fact which explains the observed larger particle sizes for lower concentrations obtained in procedure A compared to B. It is thus important to measure the particle size within each synthesized sample, as small variations in the sol-gel process can lead to quite different results.

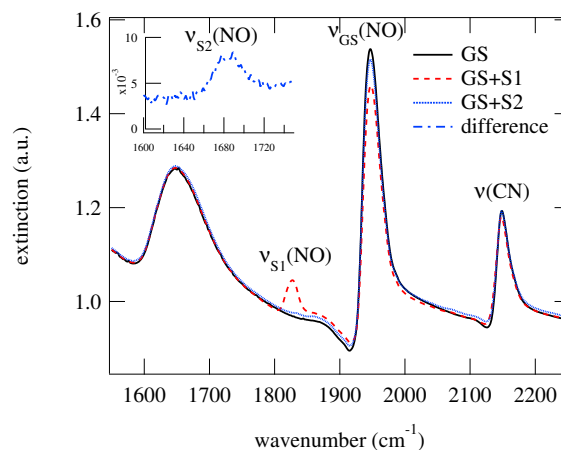


Fig. 3 Infrared spectra at $T = 80 \text{ K}$ of a SNP xerogel in GS and after irradiation with 458 nm and 1064 nm for S1 and S2, respectively.

3.2 Properties of linkage isomers

Infrared spectroscopy is a fast and efficient tool to identify the photoinduced linkage isomers, which is suitable also for the characterization of molecules embedded in silica matrices¹¹. Fig. 3 shows the infrared spectra collected at 80K in the range $1550\text{--}2250 \text{ cm}^{-1}$ in a gel with $375 \mu\text{mol}$ SNP that was synthesized along procedure B. This corresponds to a concentration where SNP is embedded as isolated complex in the pores of the silica matrix. In the GS we can clearly identify the $\nu(\text{NO})$ and $\nu(\text{CN})$ stretching vibrations at 1947 and 2149 cm^{-1} , respectively. The band at 1650 cm^{-1} is the deformation mode $\delta(\text{H}_2\text{O})$ of water, which is very broad due to the disordered position of the H_2O molecules and possibly the presence of hydrogen bonds within the pores. Compared to crystalline SNP, where the $\nu(\text{NO})$ and $\nu(\text{CN})$ stretching vibrations are found at 1947 and 2147 cm^{-1} , respectively⁴², no significant shifts are observed. However the fourfold splitting of the $\nu(\text{CN})$ stretching vibrations ($2147, 2163, 2168, 2177 \text{ cm}^{-1}$) present in crystalline SNP has disappeared in the gel. This and the broadening of all vibrations is due to the lack of the crystalline environment in the gel and a consequence of the disordered arrangement and environment of isolated molecules in the mesopores of the xerogel.

The illumination with 458 nm at 80 K generates the metastable state S1, which can be identified by the new $\nu(\text{NO})$ band appearing at 1828 cm^{-1} . The decrease of the area of the GS band at 1947 cm^{-1} yields the amount of transferred molecules, i.e. the population of S1, of 17%. A subsequent illumination with 1064 nm transfers the molecules from S1 towards S2 and partially back to GS. As can be seen from Fig. 3 the S1 band disappears and the GS band increases. The new band of S2 is hidden in the H_2O absorption band, but can be identified from a difference spectrum, shown as an in-

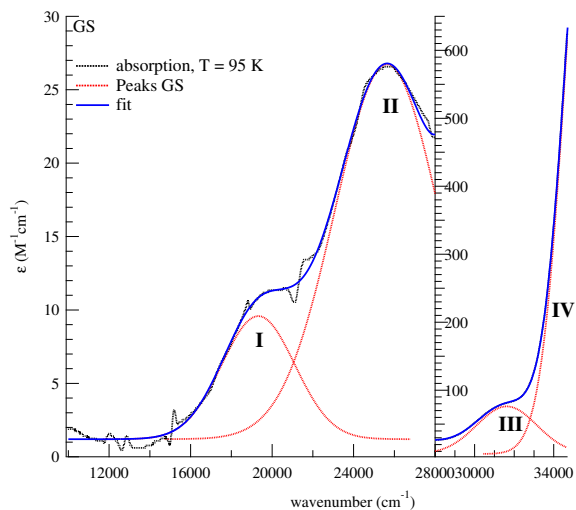


Fig. 4 Absorption spectrum of SNP embedded in Silica xerogels at 95 K. The concentrations of SNP are 400 μmol (left) and 62.5 μmol (right), such that SNP is embedded in the form of isolated complexes in the mesopores of the silica host. The dotted curves I-IV denote the Gaussian deconvolution of the spectrum.

set. The band of S2 is found at 1684 cm^{-1} and the population determined from the GS area is about 7%. Compared to the crystalline SNP, where the $\nu(\text{NO})$ stretching vibrations of S1 and S2 are found at 1835 and 1664 cm^{-1} , respectively, we observe a shift of 7 and 20 cm^{-1} for S1 and S2, respectively. The large width of the two bands in the xerogel samples of 40 and 60 cm^{-1} for S1 and S2, is a clear hint for the disordered arrangement of the molecules within the pores and possibly weak interactions with the matrix, e.g. with OH groups on the pore surfaces. In general we could expect that S2 with its side-on position reacts more sensitively on small local structural changes that could occur in the isolated complexes in the gel compared to the crystalline packing²¹, which might explain the more pronounced broadening. The population of 17% is in the range of the population achieved in powder samples indicating that the molecules are statistically distributed with their fourfold axes.

UV-Vis absorption spectroscopy delivers information about the electronic structure of the compound in its different configurations. In the case of photoinduced metastable linkage isomers, the low temperature measurements yield in addition information about the spectral ranges for photoswitching⁴³. Fig. 4 shows the absorption spectra in the GS at 95 K for two SNP silica xerogel hybrids. Both have concentrations below the threshold for nanoparticle formation, i.e. less than 500 μmol SNP per gel synthesized according to procedure B. The left part of Fig. 4 shows the absorption spectrum of a 400 μmol SNP gel with the two absorption bands

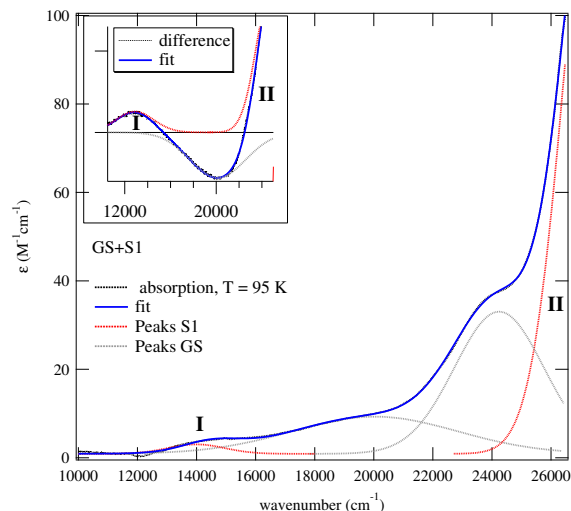


Fig. 5 Absorption spectrum of GS+S1 after illumination with 488 nm at $T=95\text{K}$. I and II denote novel absorption bands due to the generation of S1. The inset shows the difference spectrum (GS+S1)-GS.

at 19300 cm^{-1} (I) and 25600 cm^{-1} (II) with molar extinction coefficients of $\epsilon(\text{I}) = 8 \text{ M}^{-1}\text{cm}^{-1}$ and $\epsilon(\text{II}) = 25 \text{ M}^{-1}\text{cm}^{-1}$ (deconvolution with Gaussian bands). The right hand side shows the absorption spectrum of a 62.5 μmol SNP gel for illustration of the high-energy bands at 31600 cm^{-1} (III) and 37000 cm^{-1} (IV). The lower concentration simply allows for measuring up to higher energies. The molar extinction coefficients are $\epsilon(\text{III}) = 70 \text{ M}^{-1}\text{cm}^{-1}$ and $\epsilon(\text{IV}) = 900 \text{ M}^{-1}\text{cm}^{-1}$ (estimated value). For comparison the four absorption bands in crystalline SNP are found at 19800 cm^{-1} (I), 25950 cm^{-1} (II), 31750 cm^{-1} (III), and 37600 cm^{-1} (IV) for polarization along the crystallographic a -axis⁴³. There is thus only a slight redshift of maximal 500 cm^{-1} in the xerogel compared to the crystal, an effect known from SNP embedded in solutions^{44,45}. Consequently the assignment of the absorption bands to the transitions $d_{xy} \rightarrow \pi^*(\text{NO})$ (I, HOMO-LUMO), $d_{xz,yz} \rightarrow \pi^*(\text{NO})$ (II), $d_{xy} \rightarrow d_{z^2}$ (III) and $d_{xz,yz} \rightarrow d_{z^2}$ (IV) is the same as found in single crystals⁴³ and solutions⁴⁴.

In order to explore the electronic structure of S1 and S2 we performed absorption measurements at low temperature after illumination with 488 nm and subsequent illumination with 1064 nm. The results on the gel with 375 μmol SNP are shown in Figs. 5 and 6 for S1 and S2, respectively. Two bands attributed to S1 are found at 13000 cm^{-1} with $\epsilon(\text{I}) = 1.5 \text{ M}^{-1}\text{cm}^{-1}$ and at 29300 cm^{-1} with $\epsilon(\text{II}) = 640 \text{ M}^{-1}\text{cm}^{-1}$ (from fit). For S2 two bands are found at 14300 cm^{-1} with $\epsilon(\text{I}) = 0.68 \text{ M}^{-1}\text{cm}^{-1}$ and at 16200 cm^{-1} with $\epsilon(\text{II}) = 0.75 \text{ M}^{-1}\text{cm}^{-1}$ (from fit). The corresponding populations for S1 and S2 shown in Figs. 5 and 6 are 17(1)% and 6(1)%, re-

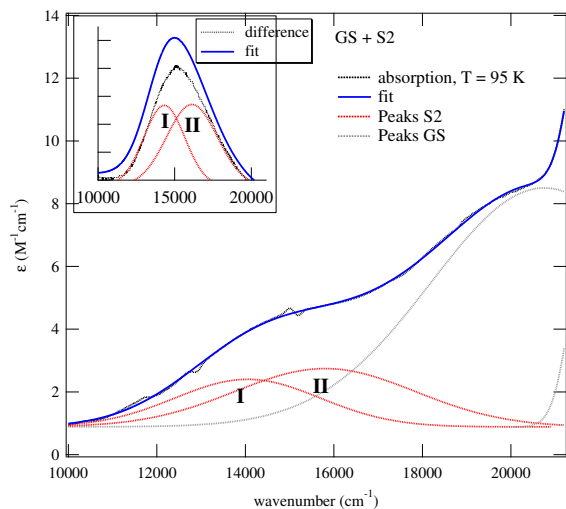


Fig. 6 Absorption spectrum of GS+S2 after illumination with 488 nm and subsequently 1064 nm at $T=95\text{K}$. I and II denote novel absorption bands due to the generation of S2. The inset shows the difference spectrum (GS+S2)-S2.

spectively. Novel bands appear in the NIR both in S1 and S2, i.e. the HOMO-LUMO transition is shifted to lower energies. This is in agreement with the single crystal study⁴³ where the corresponding transition were found at 13050cm^{-1} (I) and 29300cm^{-1} (II) for S1 and at 14000cm^{-1} (I) and 16350cm^{-1} (II) for S2 where the reduction of symmetry lifts the degeneracy of the $\pi^*(NO)$ orbital. For S1 the values are identical within errors, while for S2 a slight blueshift of the low-lying absorption at 14000cm^{-1} is observed in the gel. This apparent blueshift most probably is due to the fact that in the crystal the low-lying transition of S2 measured along the *c*-axis is found at 17000cm^{-1} and we thus would have to consider an averaged position of the transitions in the gel due to the disordered complexes. Overall we find that the generation of S1 and S2 in SNP embedded in xerogels (as isolated complexes) occurs in the same manner as in single crystals. Furthermore the electronic structure is almost identical within errors. Only small shifts of the absorption bands towards lower energies are observed, but less pronounced than found in solutions. This indicates that the electronic properties of the linkage isomers on a single molecule scale embedded in a porous host remain unaffected.

A further important characteristic of the photoinduced linkage isomers is the energy barrier that separates them from the ground state. These activation energies can be detected by Differential Scanning Calorimetry in single crystals⁴¹. Unfortunately, DSC is not applicable to the case of the low concentrations embedded in the xerogel host, because the heat-flow released is too small and blurred by the thermal isolation

properties of the surrounding host material. However, as was shown in an earlier study⁴⁶ the activation energy (for S2) can be determined by time-resolved transmission measurements after pulsed excitation at high temperatures. S2 has a lifetime in the range of 100 ns at room temperature to milliseconds at 200 K⁴⁶. We therefore performed a temperature dependent study of the lifetime of S2 excited with nanosecond laser pulses in the temperature range 200-300 K. Fig. 7 shows the temporal decay of light-induced metastable state after excitation for a pulse energy of $E = 35\text{mJ}$ at $T = 220\text{K}$ and concentrations of SNP of $310\text{ }\mu\text{mol}$ (top) and $31\text{ }\mu\text{mol}$ (bottom). For all measured temperatures the decay of $\alpha_{ii}(t)$ is mono-exponential. The open circles and squares are the thinned data points and the solid line corresponds to a fit of $\alpha_{ii}(t) = \alpha_{ii}^0 \exp(-t/\tau)$ where τ is the relaxation time (lifetime) and α_{ii}^0 is the amplitude of the light-induced absorption at $t = 0$. The amplitude of the light-induced absorption $\alpha_{ii}^0(t)$ probed at 632 nm in the xerogels is 6.3 m^{-1} and 0.8 m^{-1} for the two samples with 310 and 31 μmol SNP per gel, respectively.

From the temperature dependence of the relaxation time τ of the monoexponential decay the activation energy E_A and the frequency factor Z are obtained via the Arrhenius relation: $\tau = Z^{-1} \exp(E_A/k_B T)$. Figure 8 shows the natural logarithm of the inverse relaxation time τ^{-1} as a function of the inverse temperature for the xerogels. The linear fit yields the activation energy $E_A = 0.36(3)\text{ eV}$ and the frequency factor $Z = 1 \cdot 10^{13}\text{ s}^{-1}$ for both samples. The data and fit for lifetimes measured on a SNP single crystal are also shown in Fig. 8. For the crystal an activation energy of $E_A = 0.38(3)\text{ eV}$ and a frequency factor of $Z = 2 \cdot 10^{13}\text{ s}^{-1}$ are obtained. This shows that the size reduction to nanoparticles of 83 nm (310 μmol SNP per gel) and to single molecules in mesopores (31 μmol per gel) does not affect the activation energy and thus the potential energy surface. In comparison with an earlier study on single crystals in the temperature range 260-340 K⁴⁶ where $E_A = 0.43(3)\text{ eV}$ and $Z = 7 \cdot 10^{13}\text{ s}^{-1}$ were found, we observe a slight deviation. This can be explained by the inaccuracy of our temperature measurements (the temperature is measured on the cold finger of the cryostat). The thermal contact of the crystal sandwiched between two glass plates as well as the thermal contact of the embedded complexes through the silica xerogel to the coldfinger of the cryostat is far from being perfect. Assuming a temperature gradient yielding a 10°C higher temperature in the sample we can re-evaluate our data and find activation energies of $E_A = 0.40(3)\text{ eV}$ and $Z = 2 \cdot 10^{13}\text{ s}^{-1}$ for the two xerogel samples and $E_A = 0.42(3)\text{ eV}$ and $Z = 4 \cdot 10^{13}\text{ s}^{-1}$ for the single crystal, which corresponds perfectly to the results obtained in Ref. ⁴⁶.

Overall we find that in SNP the electronic and energetic properties of the photoinduced linkage isomers are almost identical for isolated complexes or nanoparticles embedded

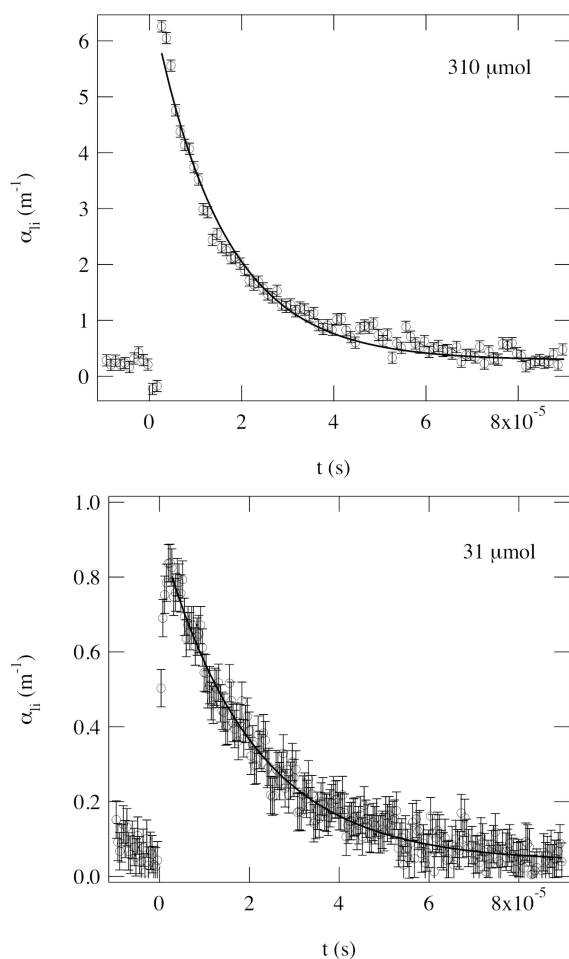


Fig. 7 Light-induced absorption $\alpha_{hi}(t)$ after pulsed excitation with nanosecond laser pulses (35 mJ/pulse at 532 nm) for two hybrid xerogels with 310 μmol (top) and 31 μmol (bottom) SNP per gel and thickness $d = 0.8$ mm and $d = 1.9$ mm, respectively. The absorption is probed at 632 nm and 220 K. The solid line corresponds to a mono-exponential fit with relaxation times $\tau = 2 \cdot 10^{-5}$ s.

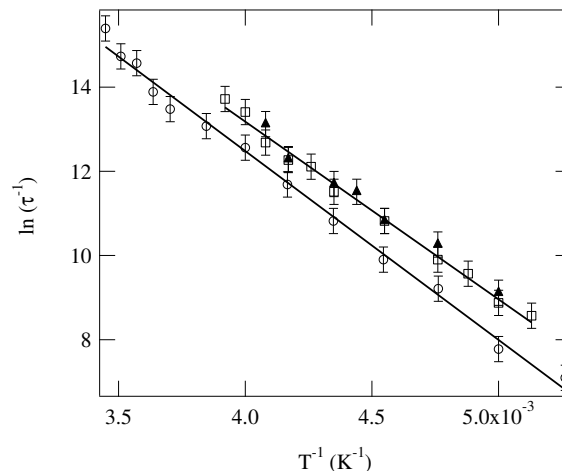


Fig. 8 Arrhenius plot of the relaxation times for two xerogels with 310 μmol (empty squares) and 31 μmol (full triangles) SNP per gel, respectively. Empty circles denote the relaxation times found in a single crystal of SNP. The absorption is probed at 632 nm. The solid line corresponds to linear fits yielding the activation energies $E_A = 0.36(3)$ eV for the xerogel hybrids and $E_A = 0.38(3)$ eV for the SNP crystal. The frequency factors are $Z = 1 \cdot 10^{13}$ s $^{-1}$ and $Z = 2 \cdot 10^{13}$ s $^{-1}$ for the xerogel hybrids and the crystal, respectively.

in xerogel matrices compared to single crystals. The activation energy and thus the lifetime of the metastable linkage isomers remains the same. The electronic transitions and especially the HOMO-LUMO transition remain unaffected as well and consequently the spectral ranges for transfer between the three NO configurations remain the same as in single crystals, except that in the gel there is no possibility to choose the polarization along a specific direction of the $[\text{Fe}(\text{CN})_5\text{NO}]$ molecule. These results underline the local nature of the linkage isomerism in these nitrosyl complexes. While the change of counter ions or of molecular composition, e.g. through the substitution of ligands, significantly affect the properties of the linkage isomers^{26–29}, the bare isolation of the complex (still with the presence of the counter ion) has nearly no influence. Furthermore this study supports the structural investigations on the relative Guanidinium nitroprusside, isolated in xerogels, where it was found that the counter ions remain at the nearly identical position with respect to the $[\text{Fe}(\text{CN})_5\text{NO}]$ molecule in the gel as in the crystal²¹. With respect to potential applications these results are encouraging, as they show us that we can produce sol-gel materials with homogeneously embedded nanoparticles or isolated molecules that retain their photosensitive properties.

4 Conclusion

We have studied the influence of the embedding of SNP in mesoporous silica xerogels on the properties of the photoinduced nitrosyl linkage isomers in SNP. Statistically distributed molecules as well as nanoparticles of SNP can be incorporated or grown in the silica matrix depending on the gelation procedures. The generation and relaxation of the metastable states as well as their electronic and nuclear structure is not significantly changed by the size of SNP particles/clusters (or local concentration of the SNP) confined in the silica matrices. In conclusion, this approach allows us to obtain photochromic nitrosyl complexes in the form of nano-objects or isolated complexes that retain their interesting properties as an internal molecular effect almost isolated from the surrounding atoms of the matrix.

References

- 1 T. Woike, W. Kirchner, G. Schetter, T. Barthel, K. Hyung-Sang and S. Haussühl, *Opt. Commun.*, 1994, **106**, 6–10.
- 2 S. Haussühl, G. Schetter and T. Woike, *Opt. Commun.*, 1995, **114**, 219–222.
- 3 T. Woike, M. Imlau, S. Haussühl, R. Rupp and R. Schieder, *Phys. Rev. B*, 1998, **58**, 8411–8415.
- 4 T. Woike, S. Haussühl, B. Sugg, R. Rupp, J. Beckers, M. Imlau and R. Schieder, *Appl. Phys. B*, 1996, **63**, 243–248.
- 5 D. Schaniel, M. Imlau, T. Weisemöller, T. Woike, K. Krämer and H. U. Güdel, *Adv. Mater.*, 2007, **19**, 723–726.
- 6 M. Goukov, D. Schaniel and T. Woike, *J. Opt. Soc. Am. B*, 2010, **27**, 927–931.
- 7 D. Levy, *Chem. Mater.*, 1997, **9**, 2666–2670.
- 8 K. Moller and T. Bein, *Chem. Mater.*, 1997, **10**, 2950–2963.
- 9 K. Ariga, *Coord. Chem. Rev.*, 2007, **251**, 2562–2591.
- 10 G. Schulz-Ekloff, D. Wöhrle, B. van Duffel and R. A. Schoonheydt, *Micro. Meso. Mat.*, 2002, **51**, 91–138.
- 11 A. Schuy, T. Woike and D. Schaniel, *J. Sol-Gel Sci. Tec.*, 2009, **50**, 403–408.
- 12 B. Cormary, I. Malfant and L. Valade, *J. Sol-Gel Sci. Tec.*, 2009, **52**, 19–23.
- 13 V. Dieckmann, M. Imlau, D. H. Taffa, L. Walder, R. Lepski, D. Schaniel and T. Woike, *Phys. Chem. Chem. Phys.*, 2010, **12**, 3283–3288.
- 14 R. Pardo, M. Zayat and D. Levy, *J. Mater. Chem.*, 2009, **19**, 6756–6760.
- 15 C. Schomburg, M. Wark, Y. Rohlfing, G. Schulz-Ekloff and D. Wöhrle, *J. Mater. Chem.*, 2001, **11**, 2014–2021.
- 16 B. Schaudel, C. Guerneur, C. Sanchez, K. Nakatani and J. A. Delaire, *J. Mater. Chem.*, 1997, **7**, 61–65.
- 17 S. Wagner, F. Leyssner, C. Kördel, S. Zarwell, R. Schmidt, M. Weinelt, K. Rück-Braun, M. Wolf and P. Tegeder, *Phys. Chem. Chem. Phys.*, 2009, **11**, 6242–6248.
- 18 P. G. Zanichelli, R. L. Sernaglia and D. W. Franco, *Langmuir*, 2006, **22**, 203–208.
- 19 F. G. Doro, U. P. Rodrigues-Filho and E. Tfouni, *J. Coll. Interface Sci.*, 2007, **307**, 405–417.
- 20 F. Chaput, J. Biteau, K. Lahlil, J. P. Boilot, B. Darracq, Y. Levy, J. Peretti, V. I. Safarov, G. Parent, A. Fernandez-Acebes and J.-M. Lehn, *Mol. Cryst. Liq. Cryst.*, 2000, **334**, 77–82.
- 21 A. Cervellino, J. Schefer, L. Keller, T. Woike and D. Schaniel, *J. Appl. Cryst.*, 2010, **43**, 1040–1045.
- 22 D. Schaniel and T. Woike, *Phys. Chem. Chem. Phys.*, 2009, **11**, 4391–4395.
- 23 D. Fomitchev, T. R. Furlani and P. Coppens, *Inorg. Chem.*, 1998, **37**, 1519–1526.
- 24 P. Schaiquevich, J. Guida and P. Aymonino, *Inorg. Chim. Acta*, 2000, **303**, 277–281.
- 25 D. Fomitchev, P. Coppens, T. Li, K. A. Bagley, L. Chen and G. B. Richter-Addo, *Chem. Commun.*, 1999, 2013–2014.
- 26 K. Ookubo, Y. Morioka, H. Tomizawa and E. Miki, *J. Mol. Struct.*, 1996, **379**, 241–247.
- 27 P. Coppens, I. Novozhilova and A. Kovalevsky, *Chem. Rev.*, 2002, **102**, 861–883.
- 28 D. Schaniel, B. Cormary, I. Malfant, L. Valade, T. Woike, B. Delley, K. Krämer and H. U. Güdel, *Phys. Chem. Chem. Phys.*, 2007, **9**, 3717–3724.
- 29 D. Schaniel, T. Woike, B. Delley, D. Biner, K. Krämer and H. U. Güdel, *Phys. Chem. Chem. Phys.*, 2005, **7**, 1164–1170.
- 30 J. Guida, O. Piro and P. Aymonino, *Inorg. Chem.*, 1995, **34**, 4113–4116.
- 31 P. Gütlich, Y. Garcia and T. Woike, *Coord. Chem. Rev.*, 2001, **219–221**, 839–879.
- 32 D. Schaniel, T. Woike, B. Delley, D. Biner, K. Krämer and H. U. Güdel, *Phys. Chem. Chem. Phys.*, 2007, **9**, 5149–5157.
- 33 D. Schaniel, T. Woike, N. R. Behrnd, J. Hauser, K. Krämer, T. Todorova and B. Delley, *Inorg. Chem.*, 2009, **48**, 11399–11406.
- 34 H. Zöllner, W. Krasser, T. Woike and S. Haussühl, *Chem. Phys. Lett.*, 1989, **161**, 497–501.
- 35 D. Schaniel, M. Nicoul and T. Woike, *Phys. Chem. Chem. Phys.*, 2010, **12**, 9029–9033.
- 36 M. Carducci, M. Pressprich and P. Coppens, *J. Am. Chem. Soc.*, 1997, **119**, 2669–2678.
- 37 D. Schaniel, J. Schefer, T. Woike and V. Petříček, *Phys. Rev. B*, 2005, **71**, 174112.
- 38 D. Schaniel, J. Schefer, T. Woike and V. Petříček, *Phys. Rev. B*, 2006, **73**, 174108.
- 39 B. Delley, J. Schefer and T. Woike, *J. Chem. Phys.*, 1997, **107**, 10067–10074.
- 40 M. Buchs, C. Daul, P. T. Manoharan and C. W. Schlöpfer, *Int. J. Quant. Chem.*, 2002, **91**, 418–431.
- 41 D. Schaniel, T. Woike, L. Tsankov and M. Imlau, *Chem. Phys.*, 2005, **429**, 19–23.
- 42 J. B. Bates and R. K. Khanna, *Inorg. Chem.*, 1970, **9**, 1376.
- 43 D. Schaniel, J. Schefer, B. Delley, M. Imlau and T. Woike, *Phys. Rev. B*, 2002, **66**, 085103.
- 44 P. Manoharan and H. Gray, *J. Am. Chem. Soc.*, 1965, **87**, 3340–3347.
- 45 M. Lynch, M. Cheng, E. Van Kuiken and M. Khalil, *J. Am. Chem. Soc.*, 2010, **133**, 5255–5262.
- 46 D. Schaniel, T. Woike, C. Merschjann and M. Imlau, *Phys. Rev. B*, 2005, **72**, 195119.